

# Ordered particle flow spontaneously generated from random thermal motion: An investigation on the second law of thermodynamics

Yu Qiao,<sup>1,2,\*</sup> Zhaoru Shang<sup>1</sup>

<sup>1</sup> Program of Materials Science and Engineering, University of California – San Diego, La Jolla, CA 92093, U.S.A.

<sup>2</sup> Department of Structural Engineering, University of California – San Diego, La Jolla, CA 92093-0085, U.S.A.

\* Email: yqiao@ucsd.edu

**Abstract:** In the current research, we show that the second law of thermodynamics can be broken by using a spontaneously nonequilibrium dimension (SND), wherein particle-particle interaction is negligible. The SND under investigation is a narrow energy barrier, with the width much less than the particle mean free path. The steady-state particle distribution across the barrier is intrinsically in a non-Boltzmann form. As a consequence, in a step-ramp model system, an ordered particle flow can be spontaneously generated from random thermal motion. When the system is isolated, entropy can decrease; if the system is in a thermal bath, useful work may be produced in a cycle through heat absorption. The overall system size can be arbitrarily large; the deviation from thermodynamic equilibrium is steady and significant; the discussion is in the framework of classical mechanics. As the concept is applied to a Fermi gas, a high specific power is predicted.

**Keywords:** Nonequilibrium steady state; Nonchaotic; The second law of thermodynamics; Monte Carlo simulation

## 1. Introduction

For more than a century, the second law of thermodynamics has been critical to many areas in physics, such as energy science and engineering, quantum mechanics, astrophysics, heat and mass transfer, to name a few [1]. However, unlike the first law of thermodynamics (conservation of energy) that is entailed by Noether's theorem [2], the second law of thermodynamics does not have a solid proof. In the classic H-theorem [3], Boltzmann mathematically constructed the principle of maximum entropy, but the derivation was based on the key assumption of molecular

chaos. If the system state is dominated by a process of little particle-particle interaction, no decisive conclusion has been reached.

Over the years, there were continued efforts to study the “counterexamples” of the second law of thermodynamics. They have hitherto demonstrated the robustness of the theory of statistical mechanics. In general, these works can be represented by two classical models: Maxwell’s demon [4,5] and Feynman’s ratchet [6]. Both of them have a variety of variants. For example, Maxwell’s demon can operate the Szilárd engine [7]; Feynman’s ratchet is somewhat equivalent to Smoluchowski’s trapdoor [8] and the “autonomous Maxwell’s demon” (i.e., the single-electron refrigerator) [9]. Maxwell’s demon is nonequilibrium, but not spontaneous; Feynman’s ratchet is spontaneous, but not nonequilibrium. Maxwell’s demon relies on external intervention to control particle behavior and, therefore, is subject to the energetic penalty associated with the physical nature of information [10,11]; in Feynman’s ratchet, the time-average behaviors of all the components are balanced.

Recently, we investigated the concept of spontaneously nonequilibrium dimension (SND), and argued that a SND-based system might not obey the second law of thermodynamics [12,13]. SND combines the nonequilibrium characteristic of Maxwell’s demon with the spontaneity of Feynman’s ratchet. One example is a narrow barrier with the width much less than the particle mean free path, so that particle-particle collision is negligible inside the SND. Across the SND, the particle distribution cannot reach thermodynamic equilibrium. Our first model system employed an energy-barrier SND [12]. The theoretical and numerical analysis suggested that useful work could be produced in a cycle by absorbing heat from a single thermal reservoir, which was attributed to the asymmetry in the cross-influence of thermally correlated thermodynamic forces. Motivated by this finding, we designed and carried out an experiment on an entropy-barrier SND [13]. The testing data demonstrated entropy decrease without energetic penalty. To adapt to these remarkable phenomena and also remain consistent with the principle of maximum entropy, the second law of thermodynamics was generalized as  $S \rightarrow S_Q$  [13], i.e., in an isolated system, entropy ( $S$ ) cannot evolve away from the maximum possible value of steady state ( $S_Q$ ). When  $S_Q$  equals to the equilibrium maximum ( $S_{eq}$ ),  $S \rightarrow S_Q$  is equivalent to the traditional entropy statement, that is, entropy of an isolated system can never decrease. When the boundary condition is changed by the SND,  $S_Q$  is reduced to the nonequilibrium maximum ( $S_{ne}$ ), so that  $S$  decreases with it.

The previous model system in [12] works in a thermal bath. It is aimed at the heat-engine statement of the second law of thermodynamics. The operation is relatively complicated, and the analysis is taxing and contains errors. The parameters must be alternately adjusted, imposing difficulties to searching for close analogs in nature or in other fields of physics. The intrinsic energy density is low. Below, we design and investigate another model system of SND. It is isolated from the environment, through which we can directly examine the entropy statement of the second law of thermodynamics. The configuration is quite simple, and its primary procedure is autonomous. We begin with discussing how local nonchaoticity may render the steady state significantly nonequilibrium (Section 2). It leads to counterintuitive effects, when implemented in a large-sized isolated step-ramp model system (Section 3), contradicting the second law of thermodynamic. Extended discussions are given in Sections 4. In Section 5, a high specific power is predicted for Fermi gas.

In this manuscript, we use “local nonchaoticity” to describe an area wherein particle-particle interaction is negligible, so that the particle trajectories inside the area tend to be nonchaotic. For the elastic-particle systems under investigation, “nonequilibrium” indicates a state of non-Boltzmann particle distribution. Unless otherwise specified, the particle distribution always refers to steady state; we are not interested in transient system behaviors. The discussions are in the framework of classical mechanics.

## **2. Nonequilibrium Steady State of a Low-Height Vertical Plane**

In this section, we analyze a locally nonchaotic energy barrier, and demonstrate that the steady-state particle distribution across it is inherently nonequilibrium. This phenomenon is incompatible with the conventional statistical mechanics. In next section, we will show that it has nontrivial consequences, when employed to form the SND in a large-sized two-ended system.

### 2.1 Locally nonchaotic energy barrier

Figure 1(A) depicts a vertical  $y$ - $z$  plane, wherein a large number of billiard-like particles randomly move. A uniform gravitational field ( $g$ ) is in the  $-z$  direction. In the two-dimensional

(2D) system, the particles are finite-sized hard disks. There is no long-range force among them. Their collision is perfectly elastic.

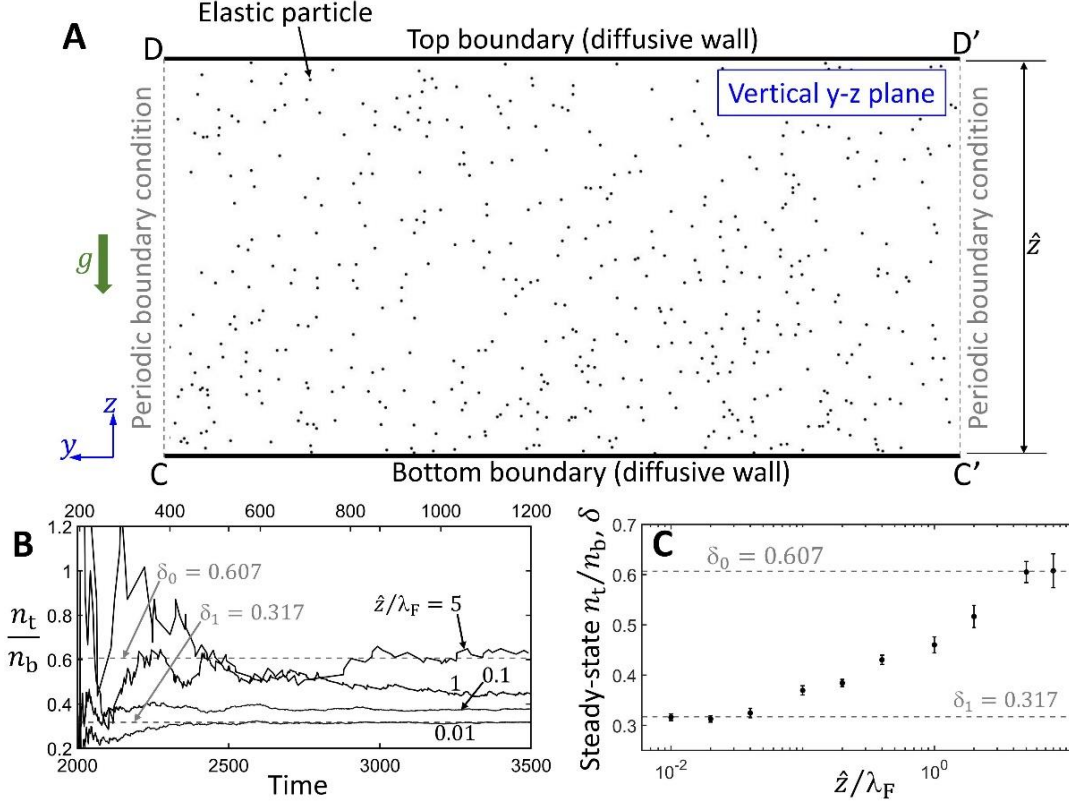


**Fig. 1** (A) A vertical y-z plane, in which a large number of elastic particles randomly move in a gravitational field ( $g$ ). (B) Typical time profiles of the  $n_t/n_b$  ratio, with  $\hat{z}/\lambda_F$  being 5, 1, 0.1, or 0.01. The upper ruler of the horizontal axis is for  $\hat{z}/\lambda_F = 0.01$ ; the lower ruler is for the other three curves. (C) The steady-state particle density ratio across the vertical plane ( $\delta$ ) as a function of  $\hat{z}/\lambda_F$ ;  $\delta$  is assessed as the steady-state  $n_t/n_b$ .

The lateral borders (DC and D'C') are open and use periodic boundary condition. The top and bottom boundaries (DD' and CC') are diffusive walls, from which the reflected particle direction is random; the reflected particle velocity is not correlated with the incident velocity, but follows the 2D Maxwell-Boltzmann distribution,  $p(v) = (mv/\bar{K})e^{-mv^2/(2\bar{K})}$ , with  $v$  being the particle velocity,  $m$  the particle mass,  $\bar{K} = k_B T$ ,  $k_B$  the Boltzmann constant, and  $T$  the nominal temperature. Here,  $T$  is defined at the system boundary, not directly related to the movement of the particles in the interior; it is mainly used as a parameter to set the boundary condition and the initial condition of computer simulation.

The upper and lower boundaries (DD' and CC') approximately represent the effects of the large horizontal areas (the plateau and the plain) that will be used in the model system in Section 3 below. A set of numerical experiments (Section A1 in Appendix) have confirmed that, as long as particle-particle collision is negligible, the main conclusion of nonequilibrium steady state is valid for a variety of different boundary conditions and initial conditions.

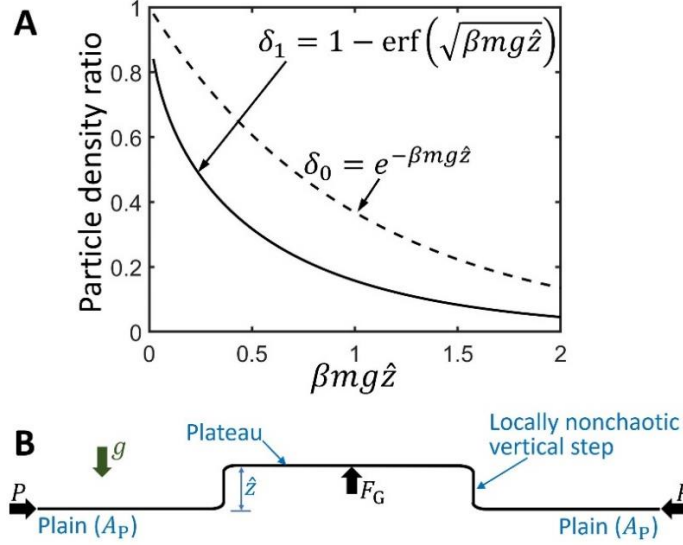


**Fig. 2 (A)** Comparison of the Boltzmann factor ( $\delta_0$ ) and the nonequilibrium steady-state particle density ratio ( $\delta_1$ ). **(B)** The vertical plane can be used to connect two large horizontal areas of different heights (the upper plateau and the lower plain) [12], in which elastic particles randomly move. A uniform gravitational field ( $g$ ) is along the vertical direction. As the step height ( $\hat{z}$ ) is much less than the nominal particle mean free path ( $\lambda_F$ ), the steady-state plateau-to-plain particle density ratio ( $\hat{\rho}$ ) tends to be close to  $\delta_1$ , significantly smaller than  $\delta_0$  (see Figure 6A below).

When the plane height ( $\hat{z}$ ) is much smaller than the nominal mean free path of the particles ( $\lambda_F$ ), the particle-particle interaction is sparse and the system state is dominated by the particle-wall collisions at DD' and CC';  $\lambda_F$  can be assessed as  $A_0/(\sqrt{8}Nd)$ , with  $A_0$  being the area of particle movement,  $N$  the total particle number, and  $d$  the particle diameter. Under this condition, as a particle moves upwards, to overcome the energy barrier of  $g$ , the y-component of particle momentum ( $p_y$ ) has little contribution; only the z-direction kinetic energy ( $K_z = mv_z^2/2$ ) is important, where  $v_z$  is the z-component of particle velocity. Define the steady-state particle density ratio across the plane as  $\delta = \rho_T/\rho_B$ , with  $\rho_T$  and  $\rho_B$  being the steady-state effective local particle

densities near the top boundary ( $z = \hat{z}$ ) and the bottom boundary ( $z = 0$ ), respectively. It may be approximately estimated as

$$\delta_1 \approx \int_{\sqrt{2g\hat{z}}}^{\infty} p_z(v_z) dv_z = 1 - \text{erf}(\sqrt{\beta mg\hat{z}}) \quad (1)$$

where  $p_z(v_z) = \sqrt{2m/(\pi K)} e^{-mv_z^2/(2K)}$  is the one-dimensional Maxwell-Boltzmann distribution of  $v_z$ , and  $\beta = 1/(k_B T)$ . In general,  $\delta_1$  is smaller than the Boltzmann factor,  $\delta_0 = e^{-\beta mg\hat{z}}$  (Figure 2A). Only when  $\hat{z}/\lambda_F \gg 1$ , with extensive particle-particle collision, would the system reach thermodynamic equilibrium, i.e.,  $\delta \rightarrow \delta_0$ ; this is consistent with that the integral of the 2D Maxwell-Boltzmann distribution of  $v$  is  $\int_{\sqrt{2g\hat{z}}}^{\infty} p(v) dv = e^{-\beta mg\hat{z}} = \delta_0$ .

## 2.2 Monte Carlo simulation

The influence of  $\hat{z}$  on  $\delta$  is visualized by a Monte Carlo (MC) simulation (Figure 1A). The computer program is available at [14]; it uses an open-source Matlab code of elastic ball collision [15]. The setup is scalable; an example of the unit system can be based on K, g/mole, Å, and fs, in which  $k_B = 8.314 \times 10^{-7}$ . The particle diameter ( $d$ ) is 1;  $A_0 = \hat{z} \cdot w_0 = 39268.75$ , where  $\hat{z} = h - d$ , and  $h$  and  $w_0$  are the height and the width of the simulation box, respectively; the total particle number  $N = 500$ ; the particle mass  $m = 1$ ; the nominal temperature  $T = 300$ . The nominal particle mean free path  $\lambda_F = A_0/(\sqrt{8}Nd) \approx 27.77$ , and the percentage of the occupied area of the particles is  $N\pi d^4/(4A_0) \approx 1\%$ .

In different simulation cases,  $\hat{z}$  is varied; the value of  $\hat{z}/\lambda_F$  ranges from 0.01 to 8. The width of the simulation box ( $w_0$ ) is changed accordingly, to keep  $A_0$  and  $\lambda_F$  constant. The gravitational acceleration ( $g$ ) is adjusted to maintain  $\beta mg\hat{z} = 0.5$ , so that  $\delta_0 = e^{-\beta mg\hat{z}} = 0.607$  and  $\delta_1 = 1 - \text{erf}(\sqrt{\beta mg\hat{z}}) = 0.317$  remain unchanged. At time zero, the particles are randomly generated in the simulation box. The probability density function of the initial particle velocity is the 2D Maxwell-Boltzmann distribution,  $p(v)$ . The initial particle direction is random.

The particle collisions are calculated by solving Newton's equations. If  $\hat{z}/\lambda_F < 1$ , the timestep of simulation ( $\Delta t_0$ ) is set to 0.0183; if  $\hat{z}/\lambda_F \geq 1$ ,  $\Delta t_0 = 0.0058$ . For each simulation case, after the settlement period ( $t_{sp} = 1.826 \times 10^3$ ), we begin to count the numbers of particle-wall collision at the top boundary DD' ( $n_t$ ) and the bottom boundary CC' ( $n_b$ ). Figure 1(B) shows

typical time profiles of the running average of the  $n_t/n_b$  ratio. The steady-state particle density ratio across the plane ( $\delta = \rho_T/\rho_B$ ) is estimated as the steady-state  $n_t/n_b$ . The total simulation time is more than  $2 \times 10^5 \Delta t_0$ , to reach the steady state. Figure 1(C) shows the calculated  $\delta$  as a function of  $\hat{z}/\lambda_F$ . For each  $\hat{z}/\lambda_F$ , three nominally same simulations are carried out, with randomized initial conditions. The error bars are the 90%-confidence interval,  $\pm 1.645 \cdot S_t/\sqrt{N_t}$ , with  $S_t$  being the standard deviation and  $N_t$  the number of data points.

When  $\hat{z} \gg \lambda_F$  (i.e., the particle-particle interaction is extensive),  $\delta \rightarrow \delta_0$ ; when  $\hat{z} \ll \lambda_F$ , (i.e., the particle-particle interaction is negligible),  $\delta \rightarrow \delta_1$ . Such a  $\delta - \hat{z}$  relationship is in agreement with [12]: The vertical plane can be used as a step to connect a large upper plateau and a large lower plain (Figure 2B), in which a large number of elastic particles randomly move in a gravitational field ( $g$ ). MC simulation has confirmed that when  $\hat{z} \ll \lambda_F$ , the steady-state plateau-to-plain particle density ratio ( $\hat{\rho} = \rho_G/\rho_P$ ) is considerably smaller than  $\delta_0$ , where  $\rho_G = N_G/A_G$  and  $\rho_P = N_P/A_P$  are the steady-state average particle densities on the plateau and the plain, respectively;  $N_G$  and  $N_P$  are the steady-state particle numbers on the plateau and the plain, respectively; and  $A_G$  and  $A_P$  are the areas of the plateau and the plain, respectively.

In the derivation of Equation (1), we do not consider the influence of the heterogeneous and anisotropic particle velocity distribution. The MC simulation result ( $\delta \approx \delta_1$  when  $\hat{z} \ll \lambda_F$ ) suggests that this simplification is acceptable, especially when  $\hat{z}/\lambda_F$  is small and the particle travel time in between the upper and lower borders tends to be short.

We tested various settings for the computer simulation (see Section A1 in Appendix). As long as there is no extensive particle-particle collision, the steady state would be significantly nonequilibrium (i.e.,  $\delta \neq \delta_0$ ), regardless of the boundary condition and the initial condition.

### 3. Large-Sized Model System

In this section, to demonstrate the nontrivial effects of the nonequilibrium steady state, we investigate a large-sized isolated model system, which consists of a locally nonchaotic energy-barrier SND similar to the vertical plane in Figure 2(A). The system has a two-ended structure, partly inspired by Feynman's ratchet.

### 3.1 Consideration on Feynman's ratchet

Feynman's ratchet is two-ended [6]. One end is a set of vanes, and the other end is a set of ratchet and pawl. They are connected through a rigid rod. Due to the random impacts of the surrounding gas molecules, the vanes undergo a rotational Brownian movement. At first glance, it seems that the ratchet might selectively guide the oscillation steps, so that the vanes are only allowed to rotate in the forward direction. Yet, such a "perpetual motion machine" would not work. To overcome the energy barrier of the pawl ( $\Delta E_p$ ), the probabilities for both of the vanes and the ratchet are governed by the same Boltzmann factor,  $e^{-\beta \cdot \Delta E_p}$ . Thus, the overall motions of the ratchet and the vanes counterbalance each other. Mere geometric asymmetry does not cause any anomalous effect.

As analyzed in Section 2, without extensive particle-particle collision, the steady state of a locally nonchaotic energy barrier may be nonequilibrium, which raises an interesting question: In a two-ended system, what would happen if one end tends to reach thermodynamic equilibrium, while the other end does not? Such a structure could be unbalanced.

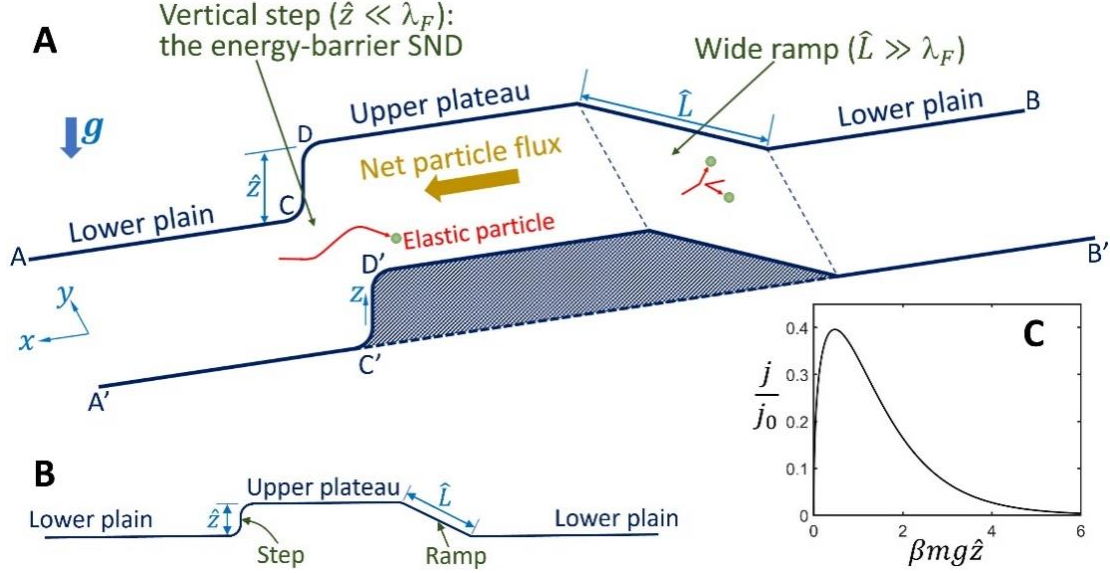
### 3.2 System design

Figure 3(A,B) depicts our model system of randomly moving elastic particles. The central area (the upper "plateau") is higher than the rest of the area (the lower "plain"). The plain and the plateau can be arbitrarily large, wherein the particle movement is ergodic and chaotic. The plateau height is  $\hat{z}$ , which is much less than  $\lambda_F$ . A uniform gravitational field ( $g$ ) is along  $-z$ , normal to the plain and the plateau. The left-hand side and the right-hand side of the plateau are connected to the plain through a vertical step and a wide ramp, respectively. The ramp size ( $\hat{L}$ ) is much larger than  $\lambda_F$ . The front and back borders (AA' and BB') are open and use periodic boundary condition; the lateral borders (AB and A'B') are rigid walls isolated from the environment.

On the one hand, since  $\hat{L} \gg \lambda_F$ , the particle collision in the ramp is extensive. Across the ramp, to maximize entropy, the steady-state particle density ratio between the plateau and the plain tends to be the Boltzmann factor [3],  $\delta_0 = e^{-\beta m g \hat{z}}$ . On the other hand, as shown in Figure 1, across



the locally nonchaotic vertical step, the particle density ratio ( $\delta$ ) tends to be  $\delta_1$ , so that the step behaves as a spontaneously nonequilibrium dimension (SND).



**Fig. 3** (A) Three-dimensional view and (B) side view of the large-sized step-ramp model system. AA' and BB' are open and use periodic boundary condition; ACDB and A'C'D'B' are rigid walls isolated from the environment. (C) The particle flow rate,  $j$ , predicted by Equation (2) ( $\tilde{A} = 1$ ).

Because  $\delta_1 < \delta_0$ , the system is unbalanced. At steady state, the overall probability for the particles to move across the ramp along  $+x$  is larger than the probability for the particles to move across the step along  $-x$ . Therefore, there would be a net particle flux ( $j$ ) in the  $+x$  direction (from the ramp side to the step side on the plateau). In essence, the SND (the low-height vertical step) plays a somewhat similar role to Maxwell's demon [4], rendering the local particle crossing ratio non-Boltzmannian; yet, it does not involve external monitoring or active control.

The net particle flux ( $j$ ) can be compared with thermodynamic equilibrium, at which the local particle density ratio across the step ( $\delta$ ) should be  $\delta_0$ . If at nonequilibrium steady state (i.e.,  $\delta \rightarrow \delta_1$ ) there were no flow (i.e.,  $j = 0$ ), since the overall system steady state (e.g.,  $j$ ) cannot be independent of the local steady-state particle distribution (e.g.,  $\delta$ ), at thermodynamic equilibrium (i.e.,  $\delta \rightarrow \delta_0$ )  $j$  has to be nonzero, which is obviously false.

For the sake of simplicity, in this section we analyze a system in which the plateau and the plain are much larger than the ramp and the step. The steady-state average particle densities on the

plateau ( $\rho_G$ ) and the plain ( $\rho_P$ ) may be assessed through  $\rho_G A_G + \rho_P A_P \approx N$  and  $\rho_G/\rho_P \approx \bar{\delta}$ , where  $\bar{\delta} = (\delta_0 + \delta_1)/2$ . Thus,  $\rho_P = N/(\bar{\delta} A_G + A_P)$ . As a first order approximation, the steady-state flow rate can be estimated as

$$j = \frac{1}{2}(\rho_P \delta_0) \bar{v}_x - \frac{1}{2}(\rho_P \delta_1) \bar{v}_x = \frac{1}{2} \frac{\bar{\rho}}{\bar{\delta} \tilde{A} + 1} \Delta \delta \cdot \bar{v}_x \quad (2)$$

where  $\bar{\rho} = N/A_P$ ,  $\Delta \delta = \delta_0 - \delta_1$ ,  $\tilde{A} = A_G/A_P$ , and  $\bar{v}_x = \sqrt{2k_B T/(\pi m)}$ . Accordingly, the steady-state drift velocity on the plain is

$$v_w = \frac{j}{\rho_P} = \frac{1}{2} \Delta \delta \cdot \bar{v}_x \quad (3)$$

Figure 3(C) shows one example of Equation (2), where  $j_0 = \bar{\rho} \cdot \bar{v}_x/2$ ,  $\bar{\rho} = N/A_0$ ,  $A_0 \approx A_G + A_P$ , and  $\tilde{A}$  is set to 1. When  $\hat{z} = 0$ , the energy barrier vanishes, so that  $j = 0$ . When the energy barrier is large, because both  $\delta_0$  and  $\delta_1$  are small, few particles are on the plateau and consequently,  $j$  is also near zero. When  $\beta m g \hat{z}$  is in the middle range,  $j$  is significant.

The net steady-state particle flow is the result of the nonequilibrium particle density ratio across the energy-barrier SND. It spontaneously comes from the random thermal movement of the particles, not subject to any energetic penalty.

### 3.3 Monte Carlo simulation of the model system

To demonstrate the concept of Figure 3, we perform a MC simulation on an isolated 2D system. The computer program is available at [14]. The simulation box represents the surface of particle movement (Figure 4A). From left to right, it contains a left plain (“+”), a step, a plateau, a wide ramp, and a right plain (“-”). The left/right borders (AA’ and BB’) are open and use periodic boundary condition. The upper and lower borders (AB and A’B’) are rigid specular walls. The simulation is scalable; an example of the unit system can be based on nm, fs, g/mol, and K, in which  $k_B = 8.314 \times 10^{-9}$ . The width of the simulation box between AB and A’B’ ( $w_0$ ) is 50. The length of each plain (“+” or “-”) is  $L_P = 5$ . The plateau length ( $L_G$ ) is 10. The step size ( $\hat{z}$ ) is 0.5. The ramp size ( $\hat{L}$ ) is 50. The total particle number  $N = 500$ ;  $d = 0.2$ ;  $m = 1$ ;  $T$  is set to 1000, which is mainly used to compute  $\beta$  and  $p(v)$  for the initial condition. The time step  $\Delta t_0 = 1$ . The nominal mean free path of the particles is  $\lambda_F = A_0/(\sqrt{8}Nd) \approx 12.46$ , much larger than  $\hat{z}$  while considerably smaller than  $\hat{L}$ .

In the step surface, from right to left, the gravitational acceleration is denoted by  $g$ . In the ramp surface, from left to right, the component of gravitational acceleration is  $\hat{z}g/\hat{L}$ . In difference simulation cases,  $g$  is adjusted, so that  $\beta mg\hat{z}$  varies from 0 to 2. There is no long-range force among the particles and the walls; the particle-particle and particle-wall collisions are elastic, calculated by Newton's equations.

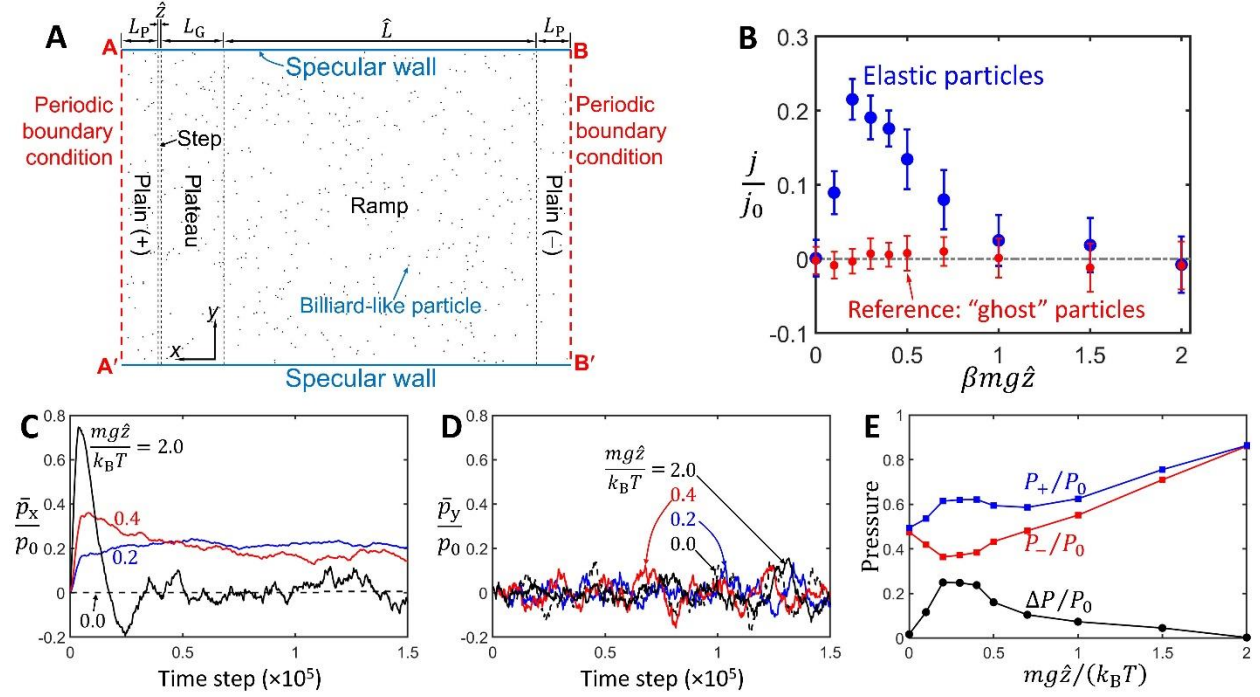


**Fig. 4** (A) The Monte Carlo simulation. (B) The calculated particle flow rate ( $j$ ) as a function of  $\beta mg\hat{z}$ . The red data points show the reference tests on “ghost” particles, with the particle-particle collision being turned off. (C) Typical time profiles of the average x-component of particle momentum ( $\bar{p}_x$ ) and (D) the average y-component of particle momentum ( $\bar{p}_y$ ). (E) The inner pressure at the left/right border (AA' and BB'), where  $P_0 = Nk_B T/A_0$ .

Initially, the particles are uniformly placed on the plain. It has been shown that the initial spatial distribution of the particles does not affect the steady state (see Section A2 in Appendix). The initial particle velocities are randomly assigned, following  $p(v)$ ; the initial particle directions are random. If the total initial x-component of momentum of all the particles is larger than  $10^{-3}p_0$ , the configuration would be rejected, where  $p_0 = \sqrt{2mk_B T/\pi}$ .

Each time when a particle crosses the left/right periodic boundary (AA' and BB'), the time, the velocity, and the direction are recorded. The average particle flow rate ( $j$ ) is calculated as

$(n_+ - n_-)/(w_0\Delta t)$  for every  $\Delta t = 5000$  timesteps (Figure 4B), where  $n_+$  and  $n_-$  are the numbers of the crossing events from plain “+” to “-” and from plain “-” to “+”, respectively. The error bars are the 90%-confidence interval. Reference tests are performed on “ghost” particles, with the particle-particle collision being turned off; all the other settings remain unchanged (the particles can still be reflected by the upper/lower walls). The results are given by the red data points. It can be seen that  $j \approx 0$  for all the reference cases, indicating that particle-particle collision is a critical factor.

The average particle momentum is defined as  $\bar{p}_x = \frac{1}{N} \sum m v_x$  and  $\bar{p}_y = \frac{1}{N} \sum m v_y$ , where  $\Sigma$  indicates summation for all the particles, and  $v_x$  and  $v_y$  are the x-component and the y-component of particle velocity, respectively. The time-average  $\bar{p}_x$  and  $\bar{p}_y$  are computed for every 200 timesteps (Figure 4C,D).

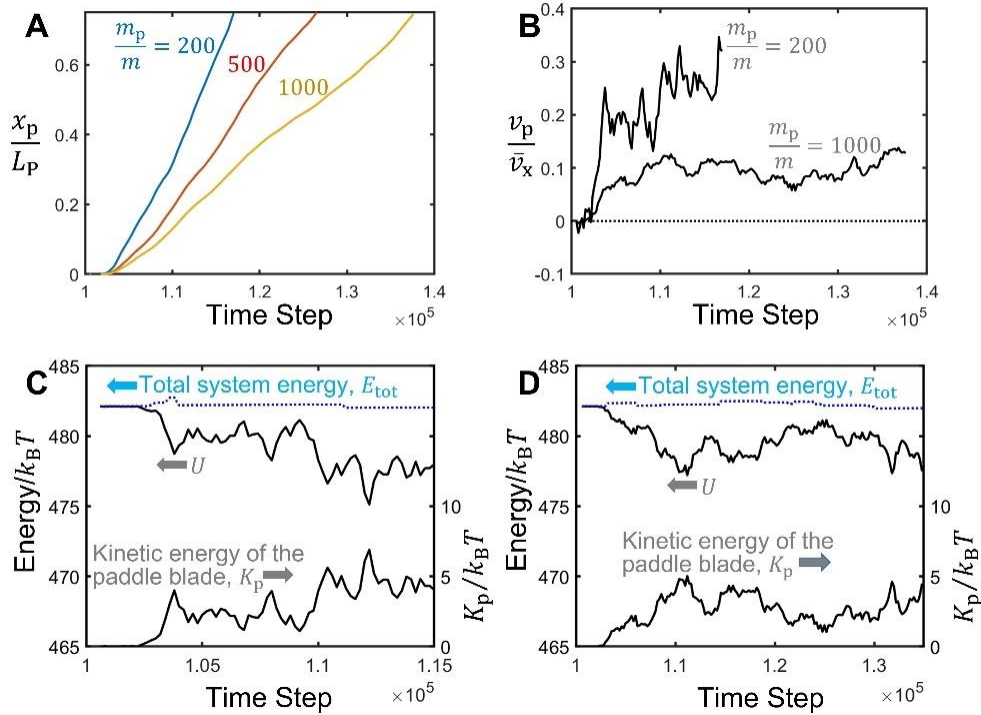


**Fig. 5** A paddle blade is driven by the particle flux, converting thermal energy to useful work,  $K_p$ . (A) Typical time profiles of the displacement ( $x_p$ ) and (B) the velocity ( $v_p$ ) of the paddle blade. (C) Typical energy evolution when  $m_p = 200m$  and (D)  $m_p = 1000m$ .

The partial pressure is calculated as  $P_{\pm} = \frac{1}{w_0 \Delta t} \sum_{\pm} m v_x$ , where  $\Sigma_+$  and  $\Sigma_-$  indicate summation in every 5000 timesteps ( $\Delta t$ ) for the particles crossing the left/right periodic boundary (AA' and BB') from plain “+” to “-” and from plain “-” to “+”, respectively. The inner pressure is defined as  $\Delta P = P_+ - P_-$  (Figure 4E).

For  $\beta m g \hat{z} = 0.2$ , after the system reaches the steady state, a paddle blade is placed at the middle of plain “+”. It is modeled as a rigid specular line normal to the x axis, with the length of  $w_0$  and the mass ( $m_p$ ) of  $200m$ ,  $500m$ , or  $1000m$ . It can freely move along the x axis, but does not move along the y axis or rotate. Figure 5(A,B) shows that the paddle blade is driven by the particle flux. When its displacement ( $x_p$ ) exceeds  $0.5L_p$ , it crosses the left/right periodic boundary (AA' and BB') from plain “+” to “-”. Figure 5(C,D) shows the energy evolution:  $U$  is the total kinetic energy and potential energy of all the particles, and the kinetic energy of the paddle blade is  $K_p = m_p v_p^2 / 2$ , where  $v_p$  is its velocity. The increase in  $K_p$  matches the reduction in  $U$ . The overall energy,  $E_{\text{tot}} = U + K_p$ , remains constant, as it should.

## 4. Discussion

### 4.1 Entropy decrease in isolated system

Figure 4(B) qualitatively agrees with Figure 3(C). They reflect the behavior of an isolated system. The difference between them should be attributed to the large ramp area and the local anisotropy and heterogeneity in the MC simulation. In both figures, when  $\beta m g \hat{z}$  is 0.1~1, a relatively large particle flux is observed. This is compatible with Figure 4(C-E). The particle movement along the y axis is unordered, so that  $\bar{p}_y$  remains near zero. With the particle flux ( $j$ ) along +x, the steady-state  $\bar{p}_x$  is nontrivial. The change in  $\bar{p}_x$  comes from the unbalanced reaction forces on the step and the ramp. Due to the biased particle movement,  $P_+ > P_-$  and there is a significant inner pressure ( $\Delta P$ ). It serves as the driving force of the paddle blade, converting thermal energy to the useful work,  $K_p$ . If the system can exchange heat with the environment (e.g., in a thermal bath), the thermal-to-kinetic energy conversion may be operated in a cycle.

For the step-ramp system, thermodynamic equilibrium is an accessible state. When  $v_w = 0$  and the plateau-to-plain particle density ratio ( $\hat{\rho} = \rho_G/\rho_P$ ) is the Boltzmann factor ( $\delta_0$ ), entropy ( $S$ ) reaches the equilibrium maximum ( $S_{eq}$ ). If the step and the ramp are much smaller than the plain and the plateau,  $N \approx N_P + N_G$ , which leads to  $N_P = N/(\delta_0 \tilde{A} + 1)$  and  $N_G = N \delta_0 \tilde{A}/(\delta_0 \tilde{A} + 1)$ . In accordance with the entropy equation of ideal gas [3], we have

$$S_{eq} = \frac{N}{\delta_0 \tilde{A} + 1} k_B \ln \frac{A_P(\delta_0 \tilde{A} + 1)}{N} + \frac{N \delta_0 \tilde{A}}{\delta_0 \tilde{A} + 1} k_B \ln \frac{A_G(\delta_0 \tilde{A} + 1)}{N \delta_0 \tilde{A}} + N k_B \sigma_0 \quad (4)$$

where  $\sigma_0 = \ln(2\pi m k_B T)$  reflects the number of velocity states of the 2D system; the first and the second terms at the right-hand side of Equation (4) reflect the numbers of location states of the plain and the plateau, respectively.

At the nonequilibrium steady state,  $\bar{\delta} \neq \delta_0$  and  $v_w \neq 0$ , and  $S$  reaches the nonequilibrium maximum ( $S_{ne}$ ) less than  $S_{eq}$  [12,13]. As an order-of-magnitude assessment,  $S_{ne}$  can be calculated similarly to Equation (4):

$$S_{ne} = \frac{N}{\bar{\delta} \tilde{A} + 1} k_B \ln \frac{A_P(\bar{\delta} \tilde{A} + 1)}{N} + \frac{N \bar{\delta} \tilde{A}}{\bar{\delta} \tilde{A} + 1} k_B \ln \frac{A_G(\bar{\delta} \tilde{A} + 1)}{N \bar{\delta} \tilde{A}} + N k_B \sigma \quad (5)$$

where  $\sigma_0 = \ln(2\pi m k_B \hat{T})$  and  $\hat{T} = T - m v_w^2/(2k_B)$ . When an ordered particle flow is generated in an initially equilibrium system,  $S$  is reduced from  $S_{eq}$  to  $S_{ne}$ ; i.e.,  $S \rightarrow S_Q$ . The entropy decrease,  $\Delta S = S_{ne} - S_{eq}$ , is caused by the unforced thermal movement, not accompanied by an energetic penalty. It is associated with the difference of  $\bar{\delta}$  and  $\hat{T}$  from  $\delta_0$  and  $T$ . The former ( $\bar{\delta}$ ) represents the influence of the particle distribution; the latter ( $\hat{T}$ ) represents the degree of randomness of particle velocity.

It is worth noting that the system does not consume energy from the gravitational field, since the steady-state particle flux is continuous. On average, for every particle moving up the ramp, there is a particle moving down the step; vice versa. The produced work ( $K_p$ ) is from thermal energy (see Figure 5C,D).

#### 4.2 Isolation and nonequilibrium steady state

It has long been known that certain “peculiar” isolated systems cannot reach thermodynamics equilibrium, such as some nonergodic or nonchaotic particle movements [16-18].

One example is a set of non-interacting elastic particles bouncing vertically up and down in a gravitational field on a horizontal floor; the time-average or ensemble-average particle number density at height  $z$  does not follow the Boltzmann factor,  $e^{-\beta mgz}$ . Usually, people do not consider them as a violation of the second law of thermodynamics, either because thermodynamic equilibrium is not accessible, or because the system is small and/or the system behavior is trivial.

For the majority of isolated systems, the second law of thermodynamics forbids their steady states from being nonequilibrium [3]. For instance, the steady-state gas pressure across a porous membrane must be uniform, regardless of the pore size and the pore geometry [19]; otherwise, it would cause a Maxwell's-demon-type controversy [13].

Generally, particle distribution in an external force field belongs to the second category. In the conventional framework of statistical mechanics, isolation and nonequilibrium steady state are mutually exclusive. Yet, Figure 4(B) clearly demonstrates a counterexample. The entropy decrease discussed in Section 4.1 is a consequence of the nonequilibrium steady state. Even if  $j = 0$  (e.g., if both sides of the plateau are connected to the plain via low-height vertical steps), because  $\hat{z} \ll \lambda_F$  and  $\hat{\rho} \neq \delta_0$ , the steady-state entropy ( $S_Q$ ) would still be less than  $S_{eq}$ . As an initially equilibrium system approaches the nonequilibrium steady state,  $S$  spontaneously becomes smaller.

The direct cause of the nonequilibrium steady state is the lack of particle collision in the SND. It renders the molecular chaos assumption in the H-theorem inapplicable [3]. Therefore, there is no mechanism to drive entropy to reach  $S_{eq}$ .

#### 4.3 Variant of system configuration

There are a variety of ways to construct a SND-based system. The model system in [12] is a variant of Figure 3(A). It is also formed by a plateau and a plain (Figure 2B), wherein a large number of elastic particles randomly move in a gravitational field. The entire plateau-plain boundary is a vertical step. When  $\hat{z} \ll \lambda_F$ , the steady-state plateau-to-plain particle density ratio ( $\hat{\rho} = \rho_G/\rho_P$ ) is much less than  $\delta_0$  (Figure 6A). The system is immersed in a thermal bath, and operated in a 4-step isothermal cycle (Figure 6B,C): The plateau is first raised by the support force ( $F_G$ ) from  $\hat{z}_L$  to  $\hat{z}_u$  (State I to II); then, the plain area is expanded by the in-plane pressure ( $P$ ) from

$A_{\text{Pl}}$  to  $A_{\text{Pu}}$  (State II to III), followed by decrease of  $\hat{z}$  back to  $\hat{z}_L$  (State III to IV); finally,  $A_{\text{P}}$  is compressed back to  $A_{\text{Pl}}$  (State IV to I).

In accordance with equilibrium statistical mechanics, in general, for two thermally correlated thermodynamic forces ( $F_a$  and  $F_b$ ), because  $F_a = \frac{\partial \mathcal{A}}{\partial x_a}$  and  $F_b = \frac{\partial \mathcal{A}}{\partial x_b}$ ,

$$\frac{\partial F_a}{\partial x_b} = \frac{\partial F_b}{\partial x_a} = \frac{\partial^2 \mathcal{A}}{\partial x_a \partial x_b} \quad (6)$$

where  $\mathcal{A} = U - TS$  is the Helmholtz free energy,  $U$  is the internal energy, and  $x_a$  and  $x_b$  are the conjugate variables of  $F_a$  and  $F_b$ , respectively. Examples of Equation (6) include the classic Maxwell relations [20], the Nernst equation [21], the Lippman equation [21], the relationship between surface tension and electrolyte concentration [22], etc. It reflects the heat-engine statement of the second law of thermodynamics, i.e., it is impossible to produce useful work in a cycle by absorbing heat from a single thermal reservoir.

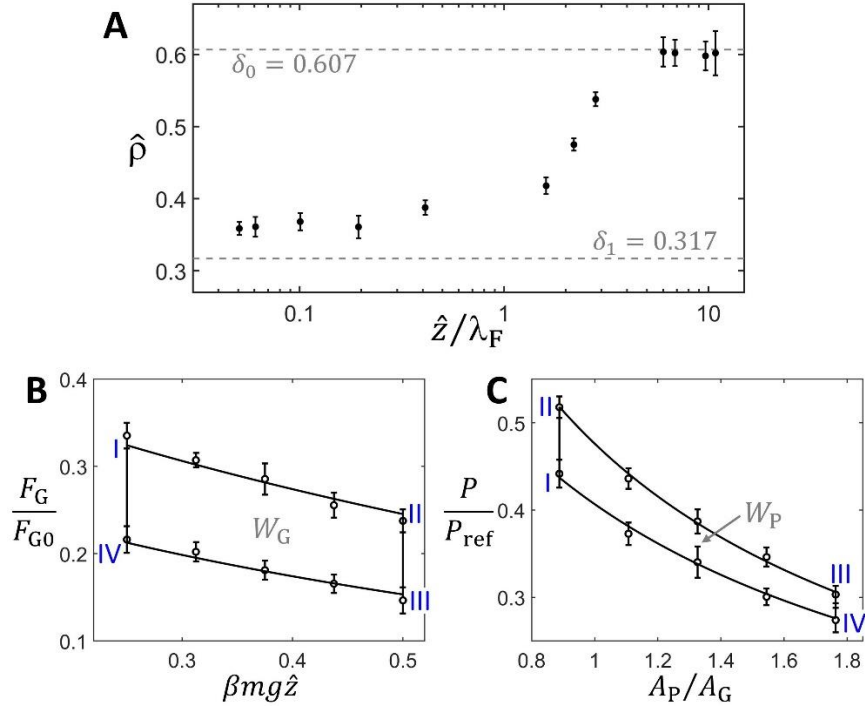


**Fig.6** MC simulation results of the plateau-plain system in Figure 2(B) [12]. **(A)** The steady-state plateau-to-plain particle density ratio ( $\hat{\rho}$ ) as a function of  $\hat{z}/\lambda_F$ . **(B)** In a 4-step isothermal cycle with  $\hat{z}/\lambda_F \approx 0.1$ , the system is changed from State I to II, III, IV, and back to I. The operation of  $F_G$  consumes work ( $W_G$ ); **(C)** the operation of  $P$  produces work ( $W_P$ ). The normalization factors are  $F_{G0} = mgN$  and  $P_{\text{ref}} = Nk_B T/A_G$ . As a consequence of the nonequilibrium steady state ( $\hat{\rho} \neq \delta_0$ ),  $W_P$  is significantly greater than  $W_G$  ( $W_P/W_G \approx 1.704$ ).



Here, we consider a system wherein the step area is negligible compared with the plain area and the plateau area. Kinetic analysis indicates that  $F_G \approx mgN_G$  and  $P \approx N_P \bar{K}/A_P$ . The conjugate variables of  $F_G$  and  $P$  are  $\hat{z}$  and  $-A_P$ , respectively. For  $F_G$  and  $P$ , Equation (6) becomes  $-\frac{\partial F_G}{\partial A_P} = \frac{\partial P}{\partial \hat{z}}$ , which leads to  $\frac{\partial \hat{P}}{\partial \hat{z}} = -\beta mg \hat{P}$ . At the nonequilibrium steady state, since  $\hat{P} \neq \delta_0$ ,  $\frac{\partial \hat{P}}{\partial \hat{z}} \neq -\beta mg \hat{P}$ , so that Equation (6) cannot be balanced, i.e.,  $\frac{\partial F_a}{\partial x_b} \neq \frac{\partial F_b}{\partial x_a}$ . As a result, in the 4-step isothermal cycle, the total work generated by  $P$  ( $W_P$ ) is greater than the total work consumed by  $F_G$  ( $W_G$ ), conflicting with the second law of thermodynamics. As  $\hat{P} \rightarrow \delta_1$ ,  $W_P > W_G$  can be observed by calculating  $W_P = N\bar{K} \cdot \ln(A_U/A_L)$  and  $W_G = mgN \cdot \int_{\hat{z}_L}^{\hat{z}_U} \left\{ \left[ 1 + 1/(\tilde{A}_I \hat{P}) \right]^{-1} - \left[ 1 + 1/(\tilde{A}_{II} \hat{P}) \right]^{-1} \right\} d\hat{z}$ , where  $A_U = (A_{Pu} + A_G \delta_u)(A_{Pl} + A_G \delta_L)$ ,  $A_L = (A_{Pl} + A_G \delta_u)(A_{Pu} + A_G \delta_L)$ ,  $\tilde{A}_I = A_G/A_{Pl}$ ,  $\tilde{A}_{II} = A_G/A_{Pu}$ ,  $\delta_u = 1 - \text{erf}(\sqrt{\beta mg \hat{z}_u})$ , and  $\delta_L = 1 - \text{erf}(\sqrt{\beta mg \hat{z}_L})$ . Figure 6(B,C) shows a MC simulation of an isothermal cycle with  $\hat{z}/\lambda_F \approx 0.1$ , the details of which are given in [12]. In Figure 6(B), the solid regression curves are based on  $F_G \approx mgN_G = mgN \hat{P} A_G / (\hat{P} A_G + A_P)$ , where  $\hat{P} = \tilde{\alpha} [1 - \text{erf}(\sqrt{\beta mg \hat{z}})]$  and  $\tilde{\alpha}$  is an adjustable parameter. For the upper curve,  $\tilde{\alpha}$  is set to 1.095; for the lower curve,  $\tilde{\alpha}$  is set to 1.185. In Figure 6(C), the solid regression curves directly use  $P \approx N_P \bar{K}/A_P = N\bar{K}/(A_P + A_G \hat{P})$ , with the average  $\hat{P}$  and the effective  $\bar{K}$  being computed from the simulation data [12]. The consumed and the produced works ( $W_G$  and  $W_P$ ) are assessed as the areas enclosed in between the upper and lower solid curves in Figure 6(B) and Figure 6(C), respectively. The numerical result confirms that  $W_P > W_G$  ( $W_P/W_G \approx 1.704$ ).

The discrepancy between  $W_P$  and  $W_G$  may also be understood through the overall system governing equations,  $PA_0 = \varepsilon_P N k_B T$  and  $F_G = \varepsilon_G mgN$ , where  $\varepsilon_P = A_0/(A_P + \hat{P} A_G)$  and  $\varepsilon_G = 1/[1 + A_P/(\hat{P} A_G)]$ . If the plateau height is zero,  $\hat{P} = 1$ , so that  $\varepsilon_P = 1$  and  $\varepsilon_G = A_G/A_0$ ; thus, the governing equations are reduced to  $PA_0 = N k_B T$  and  $F_G = mgN A_G/A_0$ . With a nontrivial  $\hat{z}$ , at thermodynamic equilibrium,  $\hat{P} = \delta_0$ , corresponding to  $W_P = W_G$ . At nonequilibrium steady state, because  $\hat{P} < \delta_0$ ,  $P$  is larger than the equilibrium pressure, while  $F_G$  is smaller than the equilibrium support force; consequently,  $W_P$  tends to be larger than  $W_G$ .

In the previous analysis in [12],  $\hat{P}$  was expressed as  $\delta_0^{\hat{\alpha}}$ , with  $\hat{\alpha}$  being an adjustable parameter. When  $\beta mg \hat{z} = 0.5$ ,  $\delta_0^2 = 0.368$ , less than  $\delta_0$  (0.607) and somewhat close to  $\delta_1$

(0.317);  $\hat{\alpha}$  could be approximately set to 2, i.e.,  $\hat{\rho} \approx \delta_0^2$ . When  $\hat{z}/\lambda_F \approx 0.1$ , the simulation results suggested that  $\hat{\rho}$  was in between  $\delta_0$  and  $\delta_1$ , and  $\delta_0^2$  described the system behavior relatively well. It should be attributed to that the particle-particle interaction in the SND is sparse but not entirely negligible. The assumption of power law ( $\delta_0^{\hat{\alpha}}$ ) is associated with the local equilibrium condition [3]; it is not valid for a highly nonequilibrium state.

The nonequilibrium steady state is not directly governed by any Massieu potential, such as the Helmholtz free energy ( $\mathcal{A}$ ) [12]. This is the reason why, with the locally nonchaotic step (i.e., the SND), Equation (6) is irrelevant. For the model system in Figure 2(B), only when  $\hat{\rho} = \delta_0$  (i.e., the steady state is equilibrium), can  $P = -\frac{\partial \mathcal{A}}{\partial A_P}$  and  $F_G = \frac{\partial \mathcal{A}}{\partial \hat{z}}$ . If  $\hat{\rho} \rightarrow \delta_1$ ,  $F_G = mgN_G = \frac{\partial \mathcal{A}}{\partial \hat{z}} + \frac{N\tilde{A}\delta_0\Theta}{(1+\delta_1\tilde{A})^2} \sqrt{\beta mg/(\pi\hat{z})}$  and  $P = \frac{N_P k_B T}{A_P} = -\frac{\partial \mathcal{A}}{\partial A_P} - \frac{N\tilde{A}\delta_1\Theta}{A_P(1+\delta_1\tilde{A})^2}$ , where  $\Theta = mg\hat{z} + k_B T \ln \delta_1$ . The second terms at the right-hand sides of the expressions of  $P$  and  $F_G$  are caused by the nonequilibrium effects.

Nevertheless, local partition functions may be separately defined for the plain ( $\mathcal{A}_P$ ) and the plateau ( $\mathcal{A}_G$ ), excluding the SND in between them. For the plain,  $\mathcal{A}_P = N_P k_B T - TS_P$ ; for the plateau,  $\mathcal{A}_G = N_G k_B T + N_G mg\hat{z} - TS_G$ , where  $S_P = N_P k_B \cdot [\ln(eA_P/N_P) + \sigma_0]$  is the entropy of the plain and  $S_G = N_G k_B [\ln(eA_G/N_G) + \sigma_0]$  is the entropy of the plateau. It can be verified that  $-\frac{\partial \mathcal{A}_P}{\partial A_P} = \frac{N_P k_B T}{A_P} = P$  and  $\frac{\partial \mathcal{A}_G}{\partial \hat{z}} = N_G mg = F_G$ .

Both entropy and thermal energy are extensive, so that  $S = S_P + S_G$  and  $Q = Q_P + Q_G$ , where  $Q$  is the absorbed heat of the system from the environment, and  $Q_P$  and  $Q_G$  are the heat absorptions of the plain and the plateau, respectively. As the change in  $S_P$  is  $Q_P/T$  and the change in  $S_G$  is  $Q_G/T$ , for the overall system the basic principle of  $\Delta S = Q/T$  is valid, with  $\Delta S$  indicating the change in  $S$ .

## 5. High Specific Power of Fermi Gas

If the particles are air molecules, at room temperature,  $\bar{v}_x$  is  $\sim 270$  m/s. According to Equation (3), the maximum drift velocity is 50~60 m/s, comparable to the wind speed of a Category 5 hurricane. However, to achieve a nontrivial particle flow,  $g$  must be greater than  $10^{12}$  m/s<sup>2</sup>, around the level of neutron stars [23].

The energy barrier may be based on Coulomb force, for which the working medium can be a Fermi gas. For instance, in a metal, the Fermi velocity ( $v_F$ ) is on the scale of  $10^6$  m/s [24]. The mean free path of the conduction electrons ( $\lambda_e$ ) is 40~60 nm [25] and their density ( $\rho_e$ ) is a few  $10^9$  C/m<sup>3</sup> [24]. If a metallic nanowire or nanolayer has an asymmetric structure with a nano-step at one end and a wide slope at the other end (Figure 7), in an external electric field ( $E$ ), a diffusive current ( $I_d$ ) may be spontaneously generated, analogous to Figures 3. The nano-step size ( $\hat{z}$ ) should be much less than  $\lambda_e$ ; the slope size ( $\hat{L}$ ) should be much larger than  $\lambda_e$ . The counterpart of  $\beta m g \hat{z}$  in Figure 3(C) is  $\beta_F e_0 E \hat{z}$ , with  $\beta_F = 1/(k_B T_F)$ ,  $T_F$  the Fermi temperature, and  $e_0$  the elementary charge. To reach  $\beta_F e_0 E \hat{z} = 0.2$ , the required  $E$  is on the scale of 50 MV/m. If  $E$  is the dielectric strength of air ( $\sim 3$  MV/m),  $\beta_F e_0 E \hat{z}$  is on the scale of  $10^{-2}$ ; in Figure 4(B), when  $\beta m g \hat{z} \approx 10^{-2}$ ,  $j/j_0$  is about 5% of the peak value.

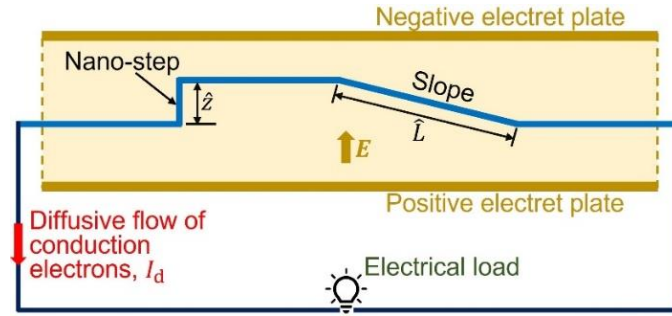


**Fig. 7.** A nonequilibrium nanowire that spontaneously produces electric energy by absorbing heat. The system is immersed in a thermal bath.

Similar to  $j_0$ , the reference current density can be set to  $j_{e0} = \rho_e v_F / 2$ , on the order of  $10^{15}$  A/m<sup>2</sup>. Figures 3(C) and 4(B) suggest that the maximum possible current density is a fraction of  $j_{e0}$ , on the order of  $10^{14}$  A/m<sup>2</sup>. For a metallic nanowire 1  $\mu$ m in length and 10 nm<sup>2</sup> in cross section, the resistance is  $10^3 \sim 10^4$   $\Omega$ , and the maximum current may be  $\sim 1$  mA. Under this condition, the upper limit of the specific power is on the order of  $10^{15}$  W/kg; the associated specific energy can be comparable to the level of nuclear reactions ( $10^7 \sim 10^8$  MJ/kg) in less than 0.1 sec. Multiple nano-steps may be placed in tandem and/or in parallel.

Besides the diffusive current, there may be other nonconventional effects of the nonequilibrium steady-state electron behavior. For example, if the “excess” conduction electrons are absorbed by surrounding atoms at the high-potential shelf and the “excess” valence electrons

are released at the low-potential shelf,  $I_d$  may be reduced. However, such a drainage effect would result in a nonuniform temperature field in the material, effectively enabling spontaneous cold-to-hot heat transfer. The dominant factors and their effectiveness remain to be seen.

## 6. Concluding Remarks and Future Study

To summarize, a locally nonchaotic energy barrier is used to form a spontaneously nonequilibrium dimension (SND) in a step-ramp system. The barrier width is much less than the nominal particle mean free path, so that particle-particle interaction is negligible inside the SND. While thermodynamic equilibrium is an accessible state, the steady state of the model system is nonequilibrium. An ordered particle flow is spontaneously generated from random thermal motion. It leads to entropy decrease in an isolated setup, which also allows for production of useful work in a cycle from a single thermal reservoir. The system contains many particles and can be arbitrarily large; the deviation from thermodynamic equilibrium is unforced, steady, and significant. Such a phenomenon breaks the second law of thermodynamics, and may be described by the generalized form ( $S \rightarrow S_Q$ ).

The current research studies the simplest possible classical mechanics models, to focus on the concept of local nonchaoticity. In addition to gravity and Coulomb force, a variety of other thermodynamic forces may also be relevant, including inertial force and magnetic momentum; in addition to the narrow energy barrier, a variety of other mechanisms may also be applicable to SND, such as switchable or distributed components [12], entropy barrier [13], etc. An important future research topic is to explore whether such spontaneous or “perpetual” particle behaviors may exist in nature, e.g., on atomic and molecular scales, on subatomic scales, in ultrahigh- $g$  environments, or with weak/sparse particle interactions. Quantum mechanical models and string theory may be analyzed. The state evolution in phase space should be examined.

## Appendix

### A1. Vertical plane: Various boundary conditions and initial conditions

We tested various boundary conditions and initial conditions for the system in Figure 1(A). As long as the particle-particle interaction is negligible in the vertical plane, the steady-state particle distribution is always nonequilibrium, regardless of the specific form of system setting.

For  $\hat{z}/\lambda_F = 0.1$ , two different initial conditions are investigated. The first is near-uniform, the same as in Section 2.2 (Figure 8A); i.e., initially, the particles are randomly placed in the plane. The second is near-equilibrium (Figure 8B); i.e., the initial probability for a particle to be placed at height  $z$  follows the Boltzmann factor,  $e^{-\beta mgz}$ . The initial particle velocity follows  $p(v)$ ; the initial particle direction is random.

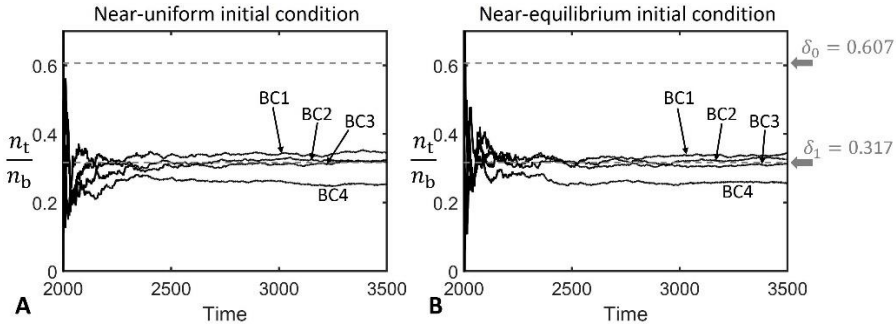


**Fig.8** Two different initial conditions are tested for  $\hat{z}/\lambda_F = 0.1$ : initially, the particles are randomly placed in the vertical plane, with the probability at height  $z$  (A) being constant, or (B) following the Boltzmann factor,  $e^{-\beta mgz}$ . For each initial condition, four different boundary conditions are tested: BC1, BC2, BC3, and BC4. In all the simulation cases, the steady-state  $n_t/n_b$  ratio (i.e., the steady-state particle density ratio across the vertical plane) is much less than the Boltzmann factor ( $\delta_0$ ).

The lateral borders (DC and D'C') are open and use periodic boundary condition. For each initial condition, we investigate four different boundary conditions at the upper/lower borders (DD' and CC'): BC1, BC2, BC3, and BC4. BC1 is the same as the boundary condition used in Section 2.2. Both of the upper and the lower borders are diffusive walls; the reflected particle direction is random; the reflected particle velocity is not correlated with the incident velocity, but follows the 2D Maxwell-Boltzmann distribution,  $p(v)$ . BC2 and BC3 have the same bottom boundary

condition as that of BC1. The top boundary of BC2 is a diffusive wall, while the reflected particle velocity is the same as the incident velocity. The top boundary of BC3 is a specular wall. In BC4, both of the upper and the lower boundaries are the same diffusive walls as the upper border of BC2; i.e., the reflected particle direction is random, and the reflected particle velocity equals to the incident velocity.

All the other parameters and the simulation procedure are the same as in Section 2.2. Figure 8 shows typical time profiles of the running average of  $n_t/n_b$ ; the steady-state  $n_t/n_b$  indicates the steady-state particle density ratio across the vertical plane ( $\delta$ ). It can be seen that for all the boundary conditions and both initial conditions,  $\delta$  is significantly smaller than the Boltzmann factor,  $\delta_0$ . For BC1, BC2, and BC3,  $\delta$  is around or slightly larger than  $\delta_1$ . For BC4,  $\delta$  is smaller than  $\delta_1$ , which should be associated with the heterogenous particle velocity distribution along  $z$ .

For every boundary condition, the initial condition has little influence on the steady-state  $n_t/n_b$ . In Figure 8(B), the system always evolves from the near-equilibrium initial state to the significantly nonequilibrium steady state. With BC4, the system is isolated.

## A2. Initial condition of the step-ramp system

For the step-ramp model system in Figure 4(A), when  $\beta mg\hat{z} = 0.2$ , we modify the initial spatial distribution of the particles; all the other settings are the same as in Section 3.3. At time zero, the particles are randomly placed in the entire simulation box, with the probability at height  $z$  following  $e^{-\beta mgz}$ . The adjusted nominal temperature is  $T = 1000 - E_0/(Nk_B) = 905.1$ , so that the total system energy is similar to that of Figure 4(B), where  $E_0 = \sum mgz_i$  is the total initial potential energy of all the particles, and  $z_i$  is the initial height of the  $i$ -th particle;  $T$  is used as a parameter to calculate  $\beta$  and  $p(v)$  (for the random assignment of the initial particle velocity).

The steady-state particle flux ( $j/j_0$ ) is calculated to be  $0.2090 \pm 0.0424$ , with the data scatter indicating 90%-confidence interval. It is quite close to the result in Figure 4(B) ( $0.2129 \pm 0.0363$ ), suggesting that the initial particle distribution has little effects on the steady state. Such an initial condition is near equilibrium. As the particle flow is generated, the system, while isolated, evolves from the near-equilibrium initial state to the significantly nonequilibrium steady state.

## References

1. I. Müller. *A History of Thermodynamics* (Springer, 2007).
2. Y. Kosmann-Schwarzbach. *The Noether Theorems* (Springer, 2010).
3. M. Kardar. *Statistical Physics of Particles* (Cambridge Univ. Press, 2007)
4. H. S. Leff, A. F. Rex. *Maxwell's Demon: Entropy, Information, Computing* (Princeton Univ. Press, 1990)
5. D. V. Averin, M. Möttönen, J. P. Pekola. Maxwell's demon based on a single-electron pump. *Phys. Rev. B* **84**, 245448 (2011).
6. R. P. Feynman, R. B. Leighton, M. Sands. *The Feynman Lecture Notes on Physics*, Vol. 1, Chapt. 46 (Basic Books, 2011)
7. D. Mandal, C. Jarzynski. Work and information processing in a solvable model of Maxwell's demon. *Proc. Natl. Acad. Sci. U.S.A.* **109**, 11641 (2012)
8. P. A. Skordos, W. H. Zurek. Maxwell's demon, rectifiers, and the second law: Computer simulation of Smoluchowski's trapdoor. *Am. J. Phys.* **60**, 876 (1992).
9. J. V. Koski, A. Kutvonen, T. Ala-Nissila, J. P. Pekola. On-chip Maxwell's demon as an information-powered refrigerator. *Phys. Rev. Lett.* **115**, 260602 (2015).
10. R. Landauer. Information is inevitably physical, in *Feynman and Computation*, pp77-92 (Perseus Books, Cambridge, MA, 1998)
11. D. Mandal, C. Jarzynski. Work and information processing in a solvable model of Maxwell's demon. *Proc. Natl. Acad. Sci. U.S.A.* **109**, 11641 (2012)
12. Y. Qiao, Z. Shang. Producing useful work in a cycle by absorbing heat from a single thermal reservoir: An investigation on a locally nonchaotic energy barrier, *Physica A* (2022)  
<https://doi.org/10.1016/j.physa.2022.127105>
13. Y. Qiao, Z. Shang, R. Kou. Molecular-sized outward-swinging gate: Experiment and theoretical analysis of a locally nonchaotic barrier. *Phys. Rev. E*, **104**, 064133 (2021)  
<https://doi.org/10.1103/PhysRevE.104.064133>
14. See Supplementary Data for the computer programs used in the current research, which is also available at [http://mmrl.ucsd.edu/Z\\_Upload/Papers/ComputerPrograms\\_Flux.zip](http://mmrl.ucsd.edu/Z_Upload/Papers/ComputerPrograms_Flux.zip)

15. L. Han. *Ball Collision Simulation*. <https://www.mathworks.com/matlabcentral/fileexchange/41032-ball-collision-simulation>, Matlab Central File Exchange (2022).
16. G. Lebon, D. Jou. *Understanding Nonequilibrium Thermodynamics* (Springer, 2008)
17. A. Argun, A. Moradi, E. Pince, G. B. Bagci, A. Imparato, G. Volpe. Non-Boltzmann stationary distributions and nonequilibrium relations in active baths. *Phys. Rev. E* **94**, 062150 (2016).
18. J. R. Dorfman. *An Introduction to Chaos in Nonequilibrium Statistical Mechanics* (Cambridge University Press, Cambridge, 1999).
19. W. Pauli, Thermodynamics and the kinetic theory of gases, in *Pauli Lectures on Physics*, edited by C. P. Enz, Vol.3 (MIT Press, Cambridge, MA, 1973).
20. N. D. Hari Dass. *The Principles of Thermodynamics*. CRC Press (2013).
21. C. M. A. Brett, A. M. O. Brett. *Electrochemistry: Principles, Methods, and Applications*. Oxford University Press (1993)
22. H. Motschmann. Electrolytes at the air-water interface. In: G. Kreysa, K. Ota, R. F. Savinell (eds) *Encyclopedia of Applied Electrochemistry*. Springer, New York (2014).
23. M. Camenzind. *Compact Objects in Astrophysics* (Springer, 2016)
24. R. P. Huebener. *Conductors, Semiconductors, Superconductors* (Springer, 2016)
25. D. Gall. Electron mean free path in elemental metals. *J. Appl. Phys.* **119**, 085101 (2016)